Altered primary somatosensory neuron development in a *Pten* heterozygous model for autism spectrum disorder

Alejandra Fernandez[1‡], Nick Sarn[2], Charis Eng[2,3,4], Kevin M. Wright[1,‡]

[1]Vollum Institute, Oregon Health & Science University, Portland, OR, 97239

[2]Genomic Medicine Institute, Lerner Research Institute, Cleveland Clinic, Cleveland, OH 44195

[3]Center for Personalized Genetic Healthcare, Medical Specialties Institute, Cleveland Clinic, Cleveland, OH 44195

[4]Department of Genetics and Genome Sciences, Case Western Reserve University School of Medicine, Cleveland, OH 44106

[‡]Corresponding Authors: fernaale@ohsu.edu; wrighke@ohsu.edu

Summary

Autism spectrum disorder (ASD) is a complex neurodevelopmental disorder characterized by deficits in social interactions, repetitive behaviors, and hyper- or hyposensitivity to sensory stimuli. The mechanisms underlying the emergence of sensory features in ASD are not fully understood, but recent studies in rodent models highlight that these may result from differences in primary sensory neurons themselves. We examined sensory behaviors in a *Pten* haploinsufficient mouse model (*Pten*^{Het}) for syndromic ASD and identified elevated responses to mechanical stimuli and a higher threshold to thermal responses. Transcriptomic and *in vivo* anatomical analysis

identified alterations in subtype-specific markers of primary somatosensory neurons in *Pten*^{Het} dorsal root ganglia (DRG). These defects emerge early during DRG development and involve dysregulation of multiple signaling pathways downstream of *Pten*. Finally, we show that mice harboring an ASD-associated mutation (*Pten*^{Y69H}) also show altered expression of somatosensory neuron subtype-specific markers. Together, these results show that precise levels of *Pten* are required for proper somatosensory development and provide insight into the molecular and cellular basis of sensory abnormalities in a model for syndromic ASD.

Running Title

PTEN regulates subtype-specific sensory neuron development

Keywords:

PTEN, somatosensory neuron, neuronal differentiation, diversification, DRG, Autism Spectrum Disorder

Introduction

Altered sensory responsiveness is a defining feature of autism spectrum disorder (ASD) and has been recapitulated in animal models of ASD [1-3]. While much of the research has focused on sensory processing regions of the brain, recent advances show that altered function of primary sensory neurons is frequently seen in models for ASD. Multiple groups have reported alterations in retinal [4], auditory [5], and somatosensory circuits [1-3, 6, 7].

Despite the progress made on characterizing sensory features in animal models of ASD, how these defects emerge during development remains understudied. Somatosensory information is conveyed from the periphery to the CNS by ~15 molecularly distinct primary neuron subtypes in the dorsal root ganglia (DRG). During embryonic development, nascent DRG neurons delaminate from the neural crest, coalesce into ganglia, and innervate target tissues throughout the body. Neurotrophin signaling through Trk receptors activates multiple signaling pathways that control the survival, differentiation, and maturation of DRG neurons. One of these critical pathways is the PI3K/Akt/mTOR pathway that regulates the survival and differentiation of DRG neurons [8-12]. Phosphatase and tensin homolog (PTEN), is the primary negative regulator of this pathway [13-19]. Heterozygous mutations in *PTEN* have been identified in ~2% of all ASD cases and represent up to 20% of individuals with ASD and macrocephaly [20]. Sensory phenotypes are a common feature among PTEN-associated ASD [21].

Based on its association with ASD and its critical role in regulating an essential pathway in DRG neuron development, we examined the effects of heterozygous

24 deletion of *Pten* (*Pten*^{Het}) on primary somatosensory neurons. We find that loss of a
25 single copy of *Pten* results in alterations in multiple somatosensory behaviors. Bulk
26 RNAseq analysis of adult DRGs from *Pten*^{Het} mice indicated shifts in the proportion of
27 neuronal subtypes, which was confirmed by analyzing DRG population markers *in vivo*.
28 We find that these defects manifest at the earliest stages of DRG development and are
29 accompanied by overactivation of both mTOR and GSK3-β signaling cascades
30 downstream of PTEN. In addition, mice harboring a heterozygous ASD-associated
31 mutation that shows predominant nuclear localization (*Pten*$^{Y68H/+}$) phenocopy defects in
32 DRG marker expression [22-24], highlighting the clinical relevance of our model. Taken
33 together, these results show the contribution of PTEN signaling to molecular identity in
34 DRGs, providing insight of the consequences of PTEN mutations and their contribution
35 to sensory features seen in individuals with *PTEN*-related ASD.
36
37 **Results**
38 **Alterations in *Pten* leads to somatosensory defects**
39 Germline heterozygous mutations in *PTEN* are associated with ASD and a
40 variety of behavioral phenotypes, including repetitive behaviors, anxiety, social deficits,
41 and sensory features [25-27]. Moreover, a recent study reported alterations in itch and
42 thermal processing following homozygous deletion of *Pten* from adult DRG neurons in
43 mice [28]. However, a close examination of the somatosensory phenotypes caused by
44 germline heterozygous mutations in *Pten* mice remains to be determined. We therefore
45 used a battery of sensory assays broadly focusing on responses to mechanosensation,
46 nociception, and proprioception.

47 We first assessed mechanosensation by application of an oil droplet on the back
48 of the neck of mice to cause hair deflection. This induces a “wet dog shake (WDS)”
49 response mediated by C-type low threshold mechanoreceptors (C-LTMRs) [29]. In wild
50 type animals (WT), a single oil droplet evoked WDS at a frequency of 11 WDS in a span
51 of 5 minutes, while in *Pten*^{Het} mice, the frequency increased by 55% to 16.4 in the same
52 timeframe (**Figure 1A**). We next used an adhesive sticker removal assay, which
53 measures the animal’s ability to localize mechanical stimuli and is thought to engage
54 Aβ- and Aδ-LTMRs [30, 31]. When measuring the latency to remove the sticker, we
55 found that mutant mice displayed a significant delay, with 50% of *Pten*^{Het} mice failing to
56 remove the sticker within the 15-minute timeframe. In contrast, only one WT mouse
57 (0.06%) failed to remove the adhesive within the same timeframe (**Figure 1B**).
58 Together, these results demonstrate that *Pten*^{Het} mice display alterations in responses
59 to mechanical stimulus in hairy skin.
60 We then assessed mechanical sensitivity in glabrous skin by measuring the
61 threshold to paw withdrawal in response to calibrated Von Frey fibers applied to the
62 plantar surface of the hind paw, which is mediated by Aβ-SA LTMRs [31-33]. We found
63 the threshold of withdrawal responses to be significantly decreased in *Pten*^{Het} mice, with
64 filaments ranging between 0.4 to 1.4g eliciting a response, while responses in WT mice
65 were elicited by filaments ranging from 2 to 8g. On average, *Pten*^{Het} mice thresholds
66 were reduced by 67% (**Figure 1C**), suggesting mechanosensation hypersensitivity in
67 hind paws.
68 We then assessed responses to noxious heat stimuli using a thermal probe
69 applied to the plantar surface of the hind paw that heats at a rate of 2.5°C/sec. [33, 34].

70 WT mice consistently withdrew their paws at temperatures below 50°C. In contrast,
71 *Pten*^{Het} mutants exhibited a higher threshold close to 55°C before paw withdrawal
72 (**Figure 1D**). This suggests a higher tolerance to noxious heat in *Pten*^{Het} mice.
73 Finally, we use the accelerating rotarod task to examine proprioception in WT
74 and *Pten*^{Het} mice using the accelerating rotarod task. This assay assesses gross motor
75 coordination as well as motor skill learning [35]. We found a significant effect of
76 genotype on rotarod performance on trials conducted on days two through five, with
77 *Pten*^{Het} mice showing a reduced latency to fall compared to WT littermates (**Figure 1E**).
78 Taken together, these results provide evidence of the complex alterations in sensory
79 behaviors in mice with a germline deletion of a single copy of *Pten*, as they exhibit
80 hypersensitivity to some stimuli (oil droplet, Von Frey fiber), reduced sensitivity to other
81 stimuli (adhesive sticker, temperature), and impaired sensory-motor behaviors.
82
83 **Transcriptional profiles of DRGs are altered in *Pten*^{Het} mice**
84 A recent study showed that homozygous deletion of *Pten* from adult DRGs
85 results in altered itch behavior due to the upregulation of multiple itch-related genes
86 [28]. To more comprehensively understand how heterozygous deletion of *Pten* affects
87 gene expression in DRGs, we performed bulk RNA-sequencing (RNA-seq) of whole
88 DRGs isolated from adult *Pten*^{Het} and WT littermate control mice (**Figure 2A**). We
89 identified 285 differentially expressed genes (DEG) in *Pten*^{Het} mutant mice relative to
90 WT, with 41 genes upregulated and 244 genes downregulated (**Figure 2B and Table**
91 **S1**). Overall gene expression changes were relatively small, with most of the DEG
92 either up- or downregulated by <1.5 Log2 fold change (Log2FC) (**Figure 2C**). The

93 widespread yet relatively small change in gene expression is consistent with studies
94 that have examined the effect of single copy deletion or mutation of *Pten* in other
95 neuronal populations [24, 36]. Gene Ontology (GO) analysis of DEGs identified
96 significant changes to gene networks involved in metabolism, RNA processing, signal
97 transduction, and the ubiquitination pathway (**Figure 2D**). Surprisingly, *Pten* was slightly
98 upregulated in mutant DRG samples, potentially due to epigenetic factors or altered
99 distribution of *Pten* expression throughout DRG subtypes [37].
100 We then examined whether loss of a single copy of *Pten* affected transcriptional
101 control of specific DRG subtypes by focusing on genes enriched in each somatosensory
102 neuron subtype as defined by an available single-cell RNA seq dataset [38]. We
103 examined the top 50 enriched genes within each subtype and identified those that were
104 significantly altered in $Pten^{Het}$ mutants (**Figure 3A**). We found that about ~10% of the
105 subtype-specific markers for each neuronal subtype were differentially expressed in
106 $Pten^{Het}$ DRGs (**Figure 3B**). We used DeconV, a deconvolution algorithm that leverages
107 gene expression profiles from a reference sample along with probability distributions, to
108 infer the proportional abundance of distinct cell types within a target bulk RNA-seq
109 sample [39] (**Figure 3C**). This approach detected a potentially altered distribution of
110 DRG subtype transcriptomes in $Pten^{Het}$ mutants when compared to controls, particularly
111 in populations of C-LTMRs, peptidergic nociceptors, and proprioceptors (**Figure 3D**).
112
113 **DRG subtype-specific marker expression is altered in $Pten^{Het}$ mice**
114 Based on the DeconV prediction of altered DRG subtype transcriptomes in
115 $Pten^{Het}$ mutants, we evaluated DRG subtype populations *in vivo*. We collected hindlimb-

116 innervating DRGs (lumbar level 3-4; L3-L4) from adult *Pten*^{Het} mutants and WT control
117 littermates and quantified the various DRG populations using subtype-specific markers
118 (**Figure 4A**). We found no difference in the total number of Isl1/2^{+} DRG neurons
119 between mutants and controls (**Figure 4B**). In contrast, we identified alterations in the
120 proportion of DRG neuron subtype-specific markers in *Pten*^{Het} mutants, with some
121 populations affected while others were spared. There was a 156% increase in Tyrosine
122 Hydroxylase positive (TH^{+}) C-LTMRs and a 56% increase in TrkC^{+} proprioceptors in
123 *Pten*^{Het} mutants. TrkA^{+} peptidergic nociceptors were reduced by 27% in *Pten*^{Het} mutants
124 relative to WT littermates, whereas IB4^{+} non-peptidergic nociceptors were unaffected.
125 On the other hand, Calbindin positive (CB^{+}) Aβ-LTMRs and TrkB^{+} Aδ-LTMRs were
126 unaffected in *Pten*^{Het} mutants (**Figure 4A, C**). These results were consistent with the
127 predictions from the transcriptomic data, and results suggest that loss of a single copy
128 of *Pten* causes alterations in DRG subtype-specific marker expression and potential
129 defects in subtype-specific diversification.
130

131 **Early DRG development is abnormal in *Pten*^{Het} mutants**

132 DRG subtype diversification begins embryonically and ultimately generates the
133 full complement of genetically and physiologically distinct subtypes of somatosensory
134 neurons (**Figure 5A**). Large/medium diameter neurons expressing TrkC and/or TrkB are
135 born first and give rise to most myelinated neurons including proprioceptors and
136 mechanoreceptors. TrkA expressing small diameter neurons are born shortly after the
137 TrkC/TrkB populations and differentiate into unmyelinated nociceptors and C-fiber
138 LTMRs [19]. We examined proportions of TrkA, TrkB, and TrkC positive neurons

139 between E10.5 and E14.5 to determine how early differentiation was affected in *Pten*^{Het}
140 mutants. We found a significant decrease in the number of TrkA^{+} neurons and a
141 significant increase in the number of TrkC^{+} neurons in *Pten*^{Het} mice compared to WT
142 littermates at all ages examined (**Figure 5B, D**). In contrast, the number of TrkB^{+}
143 neurons between E10.5-E14.5 was unaffected, in line with our results in adult mice
144 (**Figure 5C**). We also examined whether changes in cell proliferation or developmental
145 apoptosis contributed to the alterations in DRG subtype proportions using EdU birth
146 dating and activated Caspase-3 staining, respectively, and we observed no significant
147 differences in neuronal progenitor proliferation or developmental apoptosis between
148 *Pten*^{Het} mutants and WT littermates in developing DRGs (**Supplemental Figure 1**).
149 These results suggest that appropriate levels of Pten are critical for the proper
150 differentiation of DRG subtypes.
151
152 **Downstream signaling pathways are altered in *Pten*^{Het} mutants**
153 Given that *Pten* haploinsufficiency has distinct effects on developing DRG
154 subtypes, we reasoned that signaling cascades downstream of PTEN could potentially
155 be differentially impacted in population subtypes. PTEN is the primary negative
156 regulator of PI3K/AKT signaling and modulates activity of both the TSC/mTOR/S6
157 pathway and the GSK-3β/β-catenin pathway [40-42] (**Figure 6A**). We examined the
158 proportions of DRG neurons engaged in each signaling cascade at E11.5, using
159 phosphoS6 (pS6) immunostaining as a readout of TSC/mTOR pathway activity. We
160 used a *TCF/Lef:H2B-GFP* reporter mouse that provides a readout of WNT/β-catenin
161 signaling activity to examine GSK-3β/β-catenin activation [43]. We found an increased

162 proportion of Isl1^{+} neurons that were positive for both pS6 and GFP in *Pten^{Het}* mutants
163 when compared to WT (**Figure 6B, C**). Closer examination of each DRG subtype
164 revealed population-specific activation of PTEN-dependent downstream signaling. Both
165 TrkA^{+} and TrkC^{+} neuronal subtypes showed a significant increase in the proportion of
166 neurons positive for pS6, while there was no change in the proportion of pS6^{+} TrkB^{+}
167 neurons (**Figure 6D-G**). In contrast, only the TrkC^{+} population had a significantly
168 increased proportion of GFP^{+} neurons indicative of Gsk-3β/β-catenin activation. These
169 results provide evidence for subtype-specific alterations of signaling cascades due to
170 *Pten* haploinsufficiency during DRG development.
171

172 **DRG neuron diversification is abnormal in mice with an ASD-associated mutation**
173 **in *Pten***

174 Given the prevalence of *PTEN* mutations within the ASD population and the high
175 incidence of sensory phenotypes in ASD [44, 45], we examined DRG subtype markers
176 in a mouse model carrying a patient-specific *PTEN* mutation (*Pten$^{Y68H/+}$*). This mutation
177 affects the phosphatase domain and results in reduced protein stability, phosphatase
178 activity, and predominantly nuclear localization in CNS neurons [24, 46, 47]. We found
179 that *Pten$^{Y68H/+}$* mice have alterations in DRG subtype proportions that mirror our results
180 in *Pten^{Het}* mutants. There was a 79% increase in TH^{+} C-LTMRs and 96% increase in
181 TrkC^{+} neurons in *Pten$^{Y68H/+}$* mice when compared to WT littermates. The proportion of
182 TrkA^{+} peptidergic nociceptors was reduced by 50%, whereas the population of IB4^{+}
183 non-peptidergic nociceptors was unaffected. In contrast, there was no change in the
184 proportion of CB^{+} Aβ LTMRs or TrkB^{+} Aδ-LTMRs (**Figure 7A, B**). The nearly identical

185 phenotypes of *Pten*$^{Y68H/+}$ mice and *Pten*^{Het} mice highlights the clinical relevance of our
186 findings that identify a critical role for precise Pten levels in regulating DRG
187 development and the expression of subtype-specific markers.
188
189 **Discussion**
190 PTEN is the primary negative regulator of PI3K/AKT signaling and has been
191 extensively studied for its role in the development, function, and regeneration of the
192 nervous system. However, little is known about its contribution to the *in vivo*
193 development and function of peripheral somatosensory neurons in the DRG. Using a
194 combination of behavioral analysis, transcriptional profiling, and *in vivo* analysis of DRG
195 development, we have identified a critical role for *Pten* in the control of subtype-specific
196 gene profiles in primary sensory neurons. These results provide a molecular basis for
197 developmental mechanisms underlying the emergence of complex sensory alterations
198 in a mouse model for ASD.
199 *PTEN* plays a critical role in many neurodevelopmental processes [48]. *Pten*
200 heterozygous mouse mutants recapitulate many of the behavioral phenotypes seen in
201 patients with ASD, including social deficits, repetitive behaviors, and anxiety. At the
202 cellular level, this is accompanied by widespread brain overgrowth, altered scaling of
203 neuronal and glial cell populations, increased axonal branching, hyperconnectivity, and
204 decreased intrinsic excitability due to altered expression of ion channels [42, 49-51].
205 These results indicate multiple distinct mechanisms underlying the complexity of
206 behavioral phenotypes in *Pten* heterozygous models [42, 51]. A recent transcriptomic
207 analysis revealed that during cortical development, heterozygous deletion of *Pten*

208 affects downstream signaling differently in astrocytes and neurons [36]. Why some cell
209 types are more sensitive to *Pten* gene dosage than others remains a subject of current
210 investigation.

211 Our transcriptomic data (**Figure 3**) and *in vivo* analysis (**Figure 4, 7**) provide
212 evidence supporting a role for proper PTEN levels in DRG neuron subtype
213 differentiation. Notably, we see the same defects in DRG neuron diversification in both
214 $Pten^{Het}$ and $Pten^{Y68H/+}$ mice. We show that these defects arise early in development
215 (**Figure 5**) and appear to engage canonical pathways downstream of PTEN (**Figure 6**).
216 This is supported by the observation that both TSC/mTOR and GSK-3β/β-Catenin
217 signaling pathways are dysregulated in $Pten^{Het}$ DRGs. Interestingly, regulation of these
218 pathways seems to be specifically regulated in different DRG populations. In $Pten^{Het}$
219 mutants, both mTOR and GSK-3β/β-Catenin pathways are hyperactive in $TrkC^{+}$ DRG
220 neurons in $Pten^{Het}$ mutants, whereas only pS6 was significantly elevated in $TrkA^{+}$ DRG
221 neurons and both pathways appeared normal in $TrkB^{+}$ DRG neurons. This could reflect
222 intrinsic differences in how signaling pathways downstream of specific Trk receptors are
223 regulated, providing insight into why some DRG subtypes are more sensitive to
224 heterozygous deletion of *Pten*. Mutations in both TSC1/2 and β-catenin are associated
225 with ASD, but the interplay between signaling dynamics of these pathways and DRG
226 cell-fate specification remain to be determined [52, 53].

227 Somatosensory phenotypes in $Pten^{Het}$ mutants shed light into the consequences
228 of DRG developmental defects due to *Pten* signaling. Interestingly, we found a
229 correlation between behavioral abnormalities and alterations in specific DRG subtype
230 proportions. The increased frequency of wet dog shakes in $Pten^{Het}$ mice in the oil drop

231 test (**Figure 1A**) may be due to the increased density of TH$^+$ C-LTMRs (**Figure 4A, C**).
232 It is possible that an increase in C-LTMR numbers in DRGs may be accompanied by
233 increased receptive field coverage in hairy skin that causes light touch hypersensitivity
234 [54]. On the other hand, deficits in sensorimotor control (**Figure 1E**) correlate to the
235 increase in TrkC$^+$ proprioceptors in *Pten*^{Het} mutants. Proprioceptive sensory feedback is
236 required for the proper development of motor and sensory neuronal circuits and
237 coordination of locomotor activity [55, 56]. Therefore, it is possible that
238 overrepresentation of proprioceptors alters the precision of sensorimotor control in
239 *Pten*^{Het} mutants. Given the complex representation of pain responses across many
240 subtypes of multimodal nociceptors, the relationship between the higher temperature
241 threshold and underrepresentation of TrkA$^+$ neurons in *Pten*^{Het} mutants is unclear.
242 Importantly, at this point we cannot distinguish whether the changes in adult neuron
243 subtype markers are entirely due to altered populations of DRG subtypes, or due to
244 ectopic expression, misexpression, or reduced labeling from individual markers.
245 However, our embryonic data showing early changes in the populations of TrkA$^+$ and
246 TrkC$^+$ DRG lineages suggest a phenotype encompassing alterations to the genetic
247 profiles of each subtype of primary sensory neurons.
248 Our results support recent findings from rodent models showing that mutations in
249 ASD-susceptibility genes affect sensory circuit development and/or function [2, 6, 57-
250 62]. Rats with mutations in *Mecp2* show abnormal mechanical and thermal sensitivity
251 due to abnormal sensory neuron postnatal development and function [7]. Moreover,
252 deletion of *Mecp2* or *Gabrb3* in somatosensory neurons results in tactile deficits,
253 defects in social interactions, and anxiety-like behaviors, all of which are associated with

254 ASD [2]. Interestingly, the developmental timing of somatosensory dysfunction and
255 emergence of ASD-like behaviors in rodent models is tightly linked [3]. Our results in
256 this study reinforce the developmental origin of sensory defects in models for ASD.
257 Pharmacologically reducing tactile overactivity in *Mecp2* and *Shank3* mutants reduced
258 anxiety-like behaviors and some social deficits [6], suggesting that sensory contributions
259 to ASD behaviors may be amenable to therapeutic intervention. Considering that up to
260 90 percent of individuals with ASD experience some form of atypical sensory sensitivity
261 [45], additional research is needed to better understand the molecular and cellular basis
262 for these phenotypes.
263

264 **Acknowledgements**

265 We would like to thank the members of the Wright laboratory for their assistance and
266 discussion throughout the course of this study. Special thanks to Dr. Matthew Pomaville
267 for his insight and help with experimental troubleshooting. We also thank Dr. Martin
268 Riccomagno, Dr. Brian O'Roak, and Dr. Arpiar Saunders for their helpful suggestions on
269 the manuscript. This work was supported by NIH grant R01NS091027 (K.M.W.), OHSU
270 Fellowship for Diversity in Research (A.F.), Collins Medical Trust (A.F.) and NIH grant
271 K01NS116168 (A.F.). C.E. passed away during the preparation of this manuscript and
272 was the Sondra J and Stephen R Hardis Chair of Cancer Genomic Medicine at the
273 Cleveland Clinic and thanks the Ambrose Monell Foundation.

274 **Materials and Methods**

275 **Mouse lines.** All experiments were performed in accordance with OHSU IACUC
276 Protocol #IS00000539. Animals were housed in standard conditions and cared for by
277 the Department of Comparative Medicine at Oregon Health & Science University. Mice
278 were maintained in a 12-hour light/dark cycle and provided food and water *ad libitum*.
279 For experiments involving embryonic timepoints, noon on the date that a vaginal plug
280 was detected was considered E0.5. For experiments involving constitutive *Pten*
281 heterozygous mice, male *Pten*^{Het} breeders (*B6;129P2-Pten*^{tm1Mak}*/Mmjax*, MMRRC stock
282 #42059 [63]) were crossed with CD1 females to generate experimental mice on a mixed
283 genetic background. For examining phenotypes related to the patient-specific Y68H
284 *Pten* mutation, *Pten*$^{Y68H/+}$ male breeders [24] were crossed to CD1 females to generate
285 experimental mice. We examined activation of the GSK-3β/β-Catenin pathway, using
286 *Pten*^{Het} breeders crossed to a *TCF/Lef:H2B-EGFP* reporter line (*Tg(TCF/Lef1-*
287 *HIST1H2BB/EGFP)61Hadj/J*, MMRRC stock #013752 [43]). All animals were group
288 housed with littermates and maintained on a mixed genetic background. Mice of both
289 sexes were used for all experiments, and WT littermates were used as controls.
290
291 **Behavioral Assays.**
292 **Oil drop test.** Test was performed as previously described [29]. In brief, animals were
293 placed in a plexiglass box where they were allowed to acclimate and explore for 15
294 minutes. After the acclimation period, we delivered a 50μl drop of sunflower oil
295 (stabilized at room temperature) and observed behaviors for 5 minutes.
296 **Adhesive removal test.** Light touch was assessed as previously described [30]. Mice
297 were placed in a plexiglass container, and after a period of acclamation of at least 5

298 minutes, a small piece of tape (7mm diameter) was carefully placed onto the back of the
299 coat of an unrestrained mouse. The animal was observed for 15 minutes, and the
300 number of responses to the tape stimulus were recorded.
301 **Von Frey assay.** We used a Dynamic Plantar Aesthesiometer (UgoBasile), which has
302 calibrated von Frey fibers and a movable force-actuator, to measure mechanical
303 somatosensation. Animals were enclosed but unrestrained in an acrylic chamber placed
304 over a meshed floor during the duration of the experiments. The actuator was placed
305 below the paw of the animal to confer different degrees of force *via* a von Frey filament,
306 starting below threshold of detection and increasing until the paw withdrawal reflex was
307 elicited.
308 **Heat nociception.** Animals were placed in an acrylic box over a grated platform
309 unrestrained during the duration of the experiment. After a 5-minute acclimation period, a
310 blunt probe with a force of 1g was applied to the plantar surface to the animal's hindlimb.
311 The metal probe touched the paw, heating up at a rate of 2.5°C/sec to a maximum
312 temperature of 60°C. Animals were monitored and their reaction times and temperature at
313 the time of withdrawal were recorded. Testing was performed 3 times per animal, with a
314 60 second recovery time between intervals.
315
316 **Tissue preparation and RNA isolation.** For transcriptome profiling by RNA
317 sequencing, whole DRGs along the entire rostro-caudal axis from 4 animals of each
318 genotype were dissected, collected in 1.5 mL Eppendorf tubes, pelleted and snap-
319 frozen in dry ice. Frozen tissue was shipped on dry ice to Genewiz (Azenta Life
320 Sciences) for RNA sequencing. RNA sequencing workflow included RNA isolation,

321 PolyA selection-based mRNA enrichment, mRNA fragmentation and complementary
322 DNA (cDNA) synthesis. Sequencing of cDNA libraries was performed in the Illumina
323 NovaSeq platform with 2× 150–base pair (bp) read length. Reads were aligned to the
324 *Mus musculus* GRCm38 reference genome available on ENSEMBL with STAR aligner
325 v.2.5.2b.
326
327 **Bioinformatics data analysis.** DESeq2 was used for comparison of gene expression
328 levels between different sample groups. *P* values and $\log_2$ fold changes were calculated
329 using a Wald test. Genes with adjusted *P* values (P_{adj}) of <0.05 were referred as DEGs.
330 DeconV was used to deconvolute RNA-seq data and infer proportions of DRG subtypes
331 in WT and $Pten^{Het}$ [39]. DeconV consists of a reference model and a deconvolution
332 model. The reference model learns parameters from single-cell reference, which the
333 deconvolution model uses to infer optimal cell type composition of a bulk sample. We
334 used the adult dataset from Sharma et al. [38] as a single-cell reference and we
335 compiled bulk samples from Accession number GEO: GSE131230, and GSE162263
336 [64, 65] as the bulk counterpart of the reference sample. DeconV was executed with
337 scripts based on examples provided by the developers. Briefly, we fitted the bulk
338 reference model using the parameters of the single cell reference to obtain a
339 probabilistic model consisting of a discrete distribution (zero inflated negative-binomial)
340 with cell-type specific parameters for single-cell gene counts. Once the reference model
341 was fitted, the deconvolution model was used to translate expression to real bulk gene
342 expression. Based on the combination of parameters from the reference and
343 deconvolution models, we generated a reference file which was then used as a

344 template to infer subtype proportions in our bulk RNA-seq dataset. Default parameters
345 were used for fitting, modeling, and training of the algorithm.
346
347 **Tissue processing and immunolabeling.** All immunolabeling was performed on
348 cryosections following standard protocols [54]. Whole mouse embryos, from litters
349 ranging from E9.5 to E14.5, were fixed overnight at 4°C in 4% paraformaldehyde with
350 gentle agitation. For analysis of P21 DRGs, intact spinal columns were first dissected
351 and fixed overnight at 4°C in 4% paraformaldehyde. The next day, spinal columns were
352 washed in PBS for 30 minutes at room temperature, and spinal cords and attached
353 DRGs were dissected from the spinal column for further processing. All tissue was
354 cryoprotected by incubating in 15% sucrose in PBS for 1 hour, followed by 20% sucrose
355 in PBS overnight at 4°C with gentle agitation. Samples were mounted in OCT and
356 rapidly frozen in methylbutane on dry ice. 20μm consecutive sections were cut on a
357 Leica CM3050S cryostat, mounted on slides, and allowed to dry for 2 hours at room
358 temperature.
359 For immunolabeling, cryosections mounted on slides were washed 3 times for 5
360 minutes in PBS at room temperature and incubated for 1 hour in blocking solution (5%
361 v/v Normal Donkey Serum, 5% v/v DMSO, 0.25% v/v Triton X-100 in PBS). Slides were
362 then incubated in primary antibodies diluted in blocking solution overnight at 4°C in a
363 humidified staining box. Concentrations for primary antibodies are listed on Table 1.
364 Slides were then washed three times for 5 minutes in PBS and incubated for 2 hours at
365 room temperature in secondary antibodies diluted at 1:500 in blocking solution. EdU
366 incorporation was detected using Click-iT™ EdU Cell Proliferation Kit for Imaging, Alexa

367 Fluor™ 647 (Thermo Fisher Scientific, Cat#C10340). Slides were incubated in EdU
368 detection solution (100 μM Tris pH7.5, 4 mM $CuSO_4$, 5 μM sulfo-Cy5 azide, 100 mM
369 sodium ascorbate) for 30 min at RT, protected from light. Slides were washed 3 times
370 for 10 minutes in PBS, with 1:5000 Hoechst added to the second wash to label nuclei.
371 Slides were then coverslipped with Fluoromount -G and imaged.
372
373 **Proliferation assays.** A single intraperitoneal (IP) injection of EdU in sterile PBS (10μg
374 EdU/g body weight) was given to pregnant dams on one day between E9.5 and E14.5.
375 Two hours after injection, embryos were collected and fixed as described.
376
377 **Cell counts and statistical analysis.** To quantify immunoreactive DRG neurons, level
378 matched DRGs from lumbar segments were serially sectioned. For analysis of total
379 number of neurons, sections of entire DRGs were counted. For population proportions,
380 cell proliferation, and cell death assays, 10 consecutive sections of level matched DRGs
381 were counted. Sections were co-immunostained with antibodies against specific cell
382 makers and Isl1/2. The proportions of each population were calculated by dividing the
383 number of marker-positive cells over the number of total neurons in serial sections from
384 level-matched DRGs of control and mutant mice. Values were averaged for each
385 experiment, with a minimum of 3 animals of mixed sex for each genotype at each
386 timepoint and condition across different litters. The average ± SEM is reported in the
387 figures. Statistical analysis for each experiment was performed by Student's t-test. P-
388 values are reported in figure legends and results section.

Table 1: Antibodies used:

Antibody	Species	Supplier	Cat #	RRID	Concentration
Primary Antibodies					
Calbindin	Rabbit	Swant	CB 38	AB_10000340	1:1000
Tyrosine Hydroxylase (TH)	Rabbit	Millipore	AB152	AB_390204	1:1000
TrkA	Goat	Fisher (R&D Systems)	AF1056	AB_2283049	1:100
TrkB	Goat	Fisher (R&D Systems)	AF1494	AB_2155264	1:100
TrkC	Goat	Fisher (R&D Systems)	AF1404	AB_2155412	1:100
Casp3	Rabbit	Cell Signaling	9661S	AB_2341188	1:500
Parvalbumin	Rabbit	Swant	PVG213	AB_2721207	1:1000
Isl1/2	Mouse Igg2b	DHSB	39.4D5	AB_2314683	1:250
GFP	Chicken	Abcam	ab13970	AB_300798	1:1000
Secondary Antibodies					

Anti-Rabbit IgG 488	Donkey	Thermo Fisher Scientific	A-21206		1:500
Anti-Rabbit IgG 546	Donkey	ThermoFisher	A10040		1:500
Anti-Rabbit IgG 647	Donkey	ThermoFisher	A-31573		1:500
Anti-Mouse Igg2b 488	Goat	ThermoFisher	A-21141		1:500
Anti-Chicken IgY 488	Donkey	Jackson Immuno Research	NC0215979		1:500
Anti-Goat 647	Donkey	ThermoFisher	A-21447		1:500

References:

1. Huzard, D., et al., *Primary sensory neuron dysfunction underlying mechanical itch hypersensitivity in a Shank3 mouse model of autism.* bioRxiv, 2024: p. 2024.12.29.630575.
2. Orefice, L.L., et al., *Peripheral Mechanosensory Neuron Dysfunction Underlies Tactile and Behavioral Deficits in Mouse Models of ASDs.* Cell, 2016. **166**(2): p. 299-313.
3. Tasnim, A., et al., *The developmental timing of spinal touch processing alterations and its relation to ASD-associated behaviors in mouse models.* bioRxiv, 2023: p. 2023.05.09.539589.
4. Vlasits, A.L., et al., *Atypical retinal function in a mouse model of Fragile X syndrome.* bioRxiv, 2024.
5. McChesney, N., et al., *Peripheral Auditory Nerve Impairment in a Mouse Model of Syndromic Autism.* J Neurosci, 2022. **42**(42): p. 8002-8018.
6. Orefice, L.L., et al., *Targeting Peripheral Somatosensory Neurons to Improve Tactile-Related Phenotypes in ASD Models.* Cell, 2019. **178**(4): p. 867-886 e24.
7. Bhattacherjee, A., et al., *Neuronal cytoskeletal gene dysregulation and mechanical hypersensitivity in a rat model of Rett syndrome.* Proc Natl Acad Sci U S A, 2017. **114**(33): p. E6952-E6961.
8. Snider, W.D. and I. Silos-Santiago, *Dorsal root ganglion neurons require functional neurotrophin receptors for survival during development.* Philos Trans R Soc Lond B Biol Sci, 1996. **351**(1338): p. 395-403.
9. Klesse, L.J. and L.F. Parada, *p21 ras and phosphatidylinositol-3 kinase are required for survival of wild-type and NF1 mutant sensory neurons.* J Neurosci, 1998. **18**(24): p. 10420-8.
10. Datta, S.R., et al., *Akt phosphorylation of BAD couples survival signals to the cell-intrinsic death machinery.* Cell, 1997. **91**(2): p. 231-41.
11. Aksamitiene, E., A. Kiyatkin, and B.N. Kholodenko, *Cross-talk between mitogenic Ras/MAPK and survival PI3K/Akt pathways: a fine balance.* Biochem Soc Trans, 2012. **40**(1): p. 139-46.
12. Huang, E.J. and L.F. Reichardt, *Neurotrophins: roles in neuronal development and function.* Annu Rev Neurosci, 2001. **24**: p. 677-736.
13. Huang, E.J. and L.F. Reichardt, *Trk receptors: roles in neuronal signal transduction.* Annu Rev Biochem, 2003. **72**: p. 609-42.
14. Reichardt, L.F., *Neurotrophin-regulated signalling pathways.* Philos Trans R Soc Lond B Biol Sci, 2006. **361**(1473): p. 1545-64.
15. Postigo, A., et al., *Distinct requirements for TrkB and TrkC signaling in target innervation by sensory neurons.* Genes Dev, 2002. **16**(5): p. 633-45.
16. York, R.D., et al., *Role of phosphoinositide 3-kinase and endocytosis in nerve growth factor-induced extracellular signal-regulated kinase activation via Ras and Rap1.* Mol Cell Biol, 2000. **20**(21): p. 8069-83.
17. Philpott, K.L., et al., *Activated phosphatidylinositol 3-kinase and Akt kinase promote survival of superior cervical neurons.* J Cell Biol, 1997. **139**(3): p. 809-15.

18. Song, W., et al., *ProNGF induces PTEN via p75NTR to suppress Trk-mediated survival signaling in brain neurons.* J Neurosci, 2010. **30**(46): p. 15608-15.
19. Landy, M.A., M. Goyal, and H.C. Lai, *Nociceptor subtypes are born continuously over DRG development.* Dev Biol, 2021. **479**: p. 91-98.
20. Frazier, T.W., *Autism Spectrum Disorder Associated with Germline Heterozygous PTEN Mutations.* Cold Spring Harb Perspect Med, 2019. **9**(10).
21. Marco, E.J., et al., *Sensory processing in autism: a review of neurophysiologic findings.* Pediatr Res, 2011. **69**(5 Pt 2): p. 48R-54R.
22. Lobo, G.P., et al., *Germline and somatic cancer-associated mutations in the ATP-binding motifs of PTEN influence its subcellular localization and tumor suppressive function.* Hum Mol Genet, 2009. **18**(15): p. 2851-62.
23. He, X., et al., *Naturally occurring germline and tumor-associated mutations within the ATP-binding motifs of PTEN lead to oxidative damage of DNA associated with decreased nuclear p53.* Hum Mol Genet, 2011. **20**(1): p. 80-9.
24. Sarn, N., et al., *Germline nuclear-predominant Pten murine model exhibits impaired social and perseverative behavior, microglial activation, and increased oxytocinergic activity.* Mol Autism, 2021. **12**(1): p. 41.
25. Uljarevic, M., et al., *Toward better characterization of restricted and repetitive behaviors in individuals with germline heterozygous PTEN mutations.* Am J Med Genet A, 2021. **185**(11): p. 3401-3410.
26. Hansen-Kiss, E., et al., *A retrospective chart review of the features of PTEN hamartoma tumour syndrome in children.* J Med Genet, 2017. **54**(7): p. 471-478.
27. Busch, R.M., et al., *Neurobehavioral phenotype of autism spectrum disorder associated with germline heterozygous mutations in PTEN.* Transl Psychiatry, 2019. **9**(1): p. 253.
28. Hu, L., et al., *The role of PTEN in primary sensory neurons in processing itch and thermal information in mice.* Cell Rep, 2022. **39**(3): p. 110724.
29. Zhang, D., et al., *C-LTMRs mediate wet dog shakes via the spinoparabrachial pathway.* bioRxiv, 2024.
30. Bouet, V., et al., *The adhesive removal test: a sensitive method to assess sensorimotor deficits in mice.* Nat Protoc, 2009. **4**(10): p. 1560-4.
31. Abraira, V.E. and D.D. Ginty, *The sensory neurons of touch.* Neuron, 2013. **79**(4): p. 618-39.
32. Chaplan, S.R., et al., *Quantitative assessment of tactile allodynia in the rat paw.* J Neurosci Methods, 1994. **53**(1): p. 55-63.
33. Martinov, T., et al., *Measuring changes in tactile sensitivity in the hind paw of mice using an electronic von Frey apparatus.* J Vis Exp, 2013(82): p. e51212.
34. Deuis, J.R. and I. Vetter, *The thermal probe test: A novel behavioral assay to quantify thermal paw withdrawal thresholds in mice.* Temperature (Austin), 2016. **3**(2): p. 199-207.
35. Buitrago, M.M., et al., *Short and long-term motor skill learning in an accelerated rotarod training paradigm.* Neurobiol Learn Mem, 2004. **81**(3): p. 211-6.
36. Cheung, S.K.K., et al., *Neuropathological signatures revealed by transcriptomic and proteomic analysis in Pten-deficient mouse models.* Sci Rep, 2023. **13**(1): p. 6763.
37. Bergez-Hernandez, F., M. Irigoyen-Arredondo, and A. Martinez-Camberos, *A systematic review of mechanisms of PTEN gene down-regulation mediated by miRNA in prostate cancer.* Heliyon, 2024. **10**(15): p. e34950.

38. Sharma, N., et al., *The emergence of transcriptional identity in somatosensory neurons.* Nature, 2020. **577**(7790): p. 392-398.
39. Gynter, A., et al., *DeconV: Probabilistic Cell Type Deconvolution from Bulk RNA-sequencing Data.* bioRxiv, 2023: p. 2023.12.07.570524.
40. Georgescu, M.M., *PTEN Tumor Suppressor Network in PI3K-Akt Pathway Control.* Genes Cancer, 2010. **1**(12): p. 1170-7.
41. Huang, W., et al., *GSK3 beta mediates suppression of cyclin D2 expression by tumor suppressor PTEN.* Oncogene, 2007. **26**(17): p. 2471-82.
42. Chen, Y., et al., *Pten Mutations Alter Brain Growth Trajectory and Allocation of Cell Types through Elevated beta-Catenin Signaling.* J Neurosci, 2015. **35**(28): p. 10252-67.
43. Ferrer-Vaquer, A., et al., *A sensitive and bright single-cell resolution live imaging reporter of Wnt/ss-catenin signaling in the mouse.* BMC Dev Biol, 2010. **10**: p. 121.
44. Tilot, A.K., T.W. Frazier, 2nd, and C. Eng, *Balancing Proliferation and Connectivity in PTEN-associated Autism Spectrum Disorder.* Neurotherapeutics, 2015. **12**(3): p. 609-19.
45. Ben-Sasson, A., et al., *A meta-analysis of sensory modulation symptoms in individuals with autism spectrum disorders.* J Autism Dev Disord, 2009. **39**(1): p. 1-11.
46. Han, S.Y., et al., *Functional evaluation of PTEN missense mutations using in vitro phosphoinositide phosphatase assay.* Cancer Res, 2000. **60**(12): p. 3147-51.
47. Mighell, T.L., S. Evans-Dutson, and B.J. O'Roak, *A Saturation Mutagenesis Approach to Understanding PTEN Lipid Phosphatase Activity and Genotype-Phenotype Relationships.* Am J Hum Genet, 2018. **102**(5): p. 943-955.
48. Skelton, P.D., R.V. Stan, and B.W. Luikart, *The Role of PTEN in Neurodevelopment.* Mol Neuropsychiatry, 2020. **5**(Suppl 1): p. 60-71.
49. Huang, W.C., Y. Chen, and D.T. Page, *Hyperconnectivity of prefrontal cortex to amygdala projections in a mouse model of macrocephaly/autism syndrome.* Nat Commun, 2016. **7**: p. 13421.
50. Clipperton-Allen, A.E. and D.T. Page, *Pten haploinsufficient mice show broad brain overgrowth but selective impairments in autism-relevant behavioral tests.* Hum Mol Genet, 2014. **23**(13): p. 3490-505.
51. Garcia-Junco-Clemente, P., et al., *Overexpression of calcium-activated potassium channels underlies cortical dysfunction in a model of PTEN-associated autism.* Proc Natl Acad Sci U S A, 2013. **110**(45): p. 18297-302.
52. Davis, P.E., et al., *Tuberous Sclerosis: A New Frontier in Targeted Treatment of Autism.* Neurotherapeutics, 2015. **12**(3): p. 572-83.
53. Caracci, M.O., et al., *Wnt/beta-Catenin-Dependent Transcription in Autism Spectrum Disorders.* Front Mol Neurosci, 2021. **14**: p. 764756.
54. Pomaville, M.B. and K.M. Wright, *Follicle-innervating Adelta-low threshold mechanoreceptive neurons form receptive fields through homotypic competition.* Neural Dev, 2023. **18**(1): p. 2.
55. Akay, T., et al., *Degradation of mouse locomotor pattern in the absence of proprioceptive sensory feedback.* Proc Natl Acad Sci U S A, 2014. **111**(47): p. 16877-82.
56. Inacio, A.R., et al., *Sensory feedback synchronizes motor and sensory neuronal networks in the neonatal rat spinal cord.* Nat Commun, 2016. **7**: p. 13060.
57. Price, T.J. and O.K. Melemedjian, *Fragile X mental retardation protein (FMRP) and the spinal sensory system.* Results Probl Cell Differ, 2012. **54**: p. 41-59.

58. He, C.X., et al., *Tactile Defensiveness and Impaired Adaptation of Neuronal Activity in the Fmr1 Knock-Out Mouse Model of Autism.* J Neurosci, 2017. **37**(27): p. 6475-6487.
59. Chelini, G., et al., *Aberrant Somatosensory Processing and Connectivity in Mice Lacking Engrailed-2.* J Neurosci, 2019. **39**(8): p. 1525-1538.
60. Deng, P.Y., et al., *Hyperexcitability of Sensory Neurons in Fragile X Mouse Model.* Front Mol Neurosci, 2021. **14**: p. 796053.
61. Han, Q., et al., *SHANK3 Deficiency Impairs Heat Hyperalgesia and TRPV1 Signaling in Primary Sensory Neurons.* Neuron, 2016. **92**(6): p. 1279-1293.
62. Dawes, J.M., et al., *Immune or Genetic-Mediated Disruption of CASPR2 Causes Pain Hypersensitivity Due to Enhanced Primary Afferent Excitability.* Neuron, 2018. **97**(4): p. 806-822 e10.
63. Suzuki, A., et al., *High cancer susceptibility and embryonic lethality associated with mutation of the PTEN tumor suppressor gene in mice.* Curr Biol, 1998. **8**(21): p. 1169-78.
64. Zheng, Y., et al., *Deep Sequencing of Somatosensory Neurons Reveals Molecular Determinants of Intrinsic Physiological Properties.* Neuron, 2019. **103**(4): p. 598-616 e7.
65. Oliver, K.M., et al., *Molecular correlates of muscle spindle and Golgi tendon organ afferents.* Nat Commun, 2021. **12**(1): p. 1451.

Figure 1: Behavioral abnormalities in different sensory modalities in *Pten^{Het}* mutants. A) Schematic of oil droplet experiment, in which an oil drop is applied to the back of the neck of a mouse to elicit mechanosensory responses from C-LTMRs (left). Quantification of "wet dog shakes" (WDS) in *Pten* heterozygous mutants and control littermates in a 5-minute interval (right). The average number of responses in mutants is significantly increased by 55% (11.4 ±0.97 WDS in WT vs. 16.4 ±1.28 WDS in *Pten^{Het}*, n= 15 WT/ 14 *Pten^{Het}*, two-sided unpaired t test $p< 0.02$). **B)** Illustration of adhesive removal experiment (left) and quantification (right) showing an average increase in latency to remove the adhesive in *Pten^{Het}* mutants (5.73 ±0.93 min in WT vs. 10.26 ±1.34 min in *Pten^{Het}*, n= 15 WT/ 14 *Pten^{Het}*, $p< 0.01$). 1/15 WT and 7/14 *Pten^{Het}* mice failed to remove the adhesive within the 15-minute testing period. **C)** Schematic of Von Frey filament experiment to measure mechanosensory responses to skin indentation in hind paw (left). Heterozygous mutants show lower response threshold to skin indentation (right). Average force needed to elicit a response in mutants was decreased by over 75% in *Pten^{Het}* mice (4.6 ±0.57 g in WT vs. 1.54 ±0.18 g in *Pten^{Het}*, n= 15 WT/ 14 *Pten^{Het}*, $p< 0.002$). **D)** Schematic of thermal probe test (left) used to detect response to noxious heat (left). *Pten^{Het}* mice show increased threshold to thermal stimuli in hind paw when compared to controls (right, 43.82 ±1.30 °C in WT vs. 54.70 ±0.66 °C in *Pten^{Het}*, n= 15 WT/ 14 mutants, $p< 0.001$). **E)** Illustration of accelerating rotarod experiment, where sensory motor control is measured across a span of 5 days (left). Quantification (right) shows mean latency to fall per genotype. Both mutants and controls improve in latency to fall over the first 3 consecutive days of training before stabilizing at a specific level (48 s in WT vs 38 s in *Pten^{Het},* n= 15 WT/ 14 *Pten^{Het}*). On

days 2-5 there is a significant decrease in the latency to fall in *Pten*^{Het} mutants when compared to WT littermates (day 1: 25.6 ±2.6 s in WT vs 19.3 ±2.2 s in *Pten*^{Het}, $p = 0.08$; day 2: 29.9 ±3.01 s in WT vs 21.9 ± 1.7 s in *Pten*^{Het}, $p < 0.05$; day 3: 40.1 ±3.3 s in WT vs 28.9 ±3.5 s in *Pten*^{Het}, $p =< 0.05$; day 4: 39.5 ±3.5 s in WT vs 25.9 ±4.0 in *Pten*^{Het}, $p <0.02$; day 5: 37.0 ±2.7 s in WT vs 23.5 ±2.7 s in *Pten*^{Het}, $p<0.002$; *Pten*^{Het}).

Figure 2: Altered transcriptome in DRGs from *Pten*^{Het} mutants. A) Schematic of experimental design. Whole DRGs along the entire rostro-causal axis were dissected from *Pten*^{Het} mutants and WT littermates and processed for bulk RNA sequencing (RNAseq). **B)** Volcano plot highlighting genes that are significantly upregulated (41 genes, LFC > 0.3, yellow, right) and downregulated (244 genes, LFC < -0.3, turquoise, left) in *Pten*^{Het} mutants (adjusted p value < 0.05). **C)** List of top differentially expressed genes (top 5 upregulated genes on top, top 5 downregulated genes bottom). **D)** Barplot showing Gene Ontology analysis for differentially expressed genes. Bars are color-coded from blue to red based on the adjusted p-value.

Figure 3: Alterations in DRG neuron subtype-specific genes in *Pten^{Het}* mutants. A) Schematic experimental workflow to examine differential expression of DRG subtype-specific genes in RNA-seq data from *Pten^{Het}* and WT littermate mice. Analysis is focused on the major neuronal subpopulations in DRG (left), with multiple subtypes of peptidergic and non-peptidergic nociceptors combined into two clusters. Subtype-specific gene profiles were determined based on DRG subtype-specific markers from a scRNA-seq dataset [38]. The top 50 differentially expressed genes within each of the subtype-specific profiles were analyzed. **B).** Bar plot showing subtype-specific genes with differential expression between *Pten^{Het}* and WT littermate mice. Bar colors correspond to each DRG population subtype (adjusted $p < 0.05$). **C)** Computational framework to infer proportions of DRG subtypes from RNA-seq data using DeconV [39]. scRNAseq data containing expression profiles from each DRG population subtype is used as a reference dataset (left). Gene profiles for each population are extracted and the probabilistic framework of DeconV is used to estimate proportions of each subtype, based on an assumed linear-sum-property between single-cell and bulk gene expression (middle). DeconV then provides the proportions of each subtype as an output (right). **D)** Inferred quantification of DRG population subtypes in WT and *Pten^{Het}* by probabilistic cell type deconvolution. Quantification suggests alterations to distribution of C-LTMRs, peptidergic nociceptors, and proprioceptor populations in *Pten^{Het}* mutants.

Figure 4: Expression of subtype-specific markers is altered in *Pten^{Het}* mutants A) Representative images of cryosections of WT and *Pten^{Het}* adult DRGs with specific markers (Scale 100 μm). **B)** Quantification of the proportion of Isl1/2^{+} neurons shows no significant difference in the total population of neurons in *Pten^{Het}* and WT littermate DRGs (n=3, p=0.57, Student's t-test). **C)** Quantification of each major DRG neuronal subtype in WT and *Pten^{Het}* mutants. There were no significant changes in the number of Calbindin positive (CB^{+}) Aβ-LTMRs or TrkB^{+} Aδ-LTMRs (CB^{+} Aβ-LTMR: 11.5 ±1.1% in WT vs. 10.4 ±1.3% in *Pten^{Het}*, n=5, p=0.23 and TrkB^{+} 25.5±2.0% in WT vs. 23.2 ± 1.4% in *Pten^{Het}*, n=5, p=0.21, Student's t-test). Tyrosine hydroxylase positive (TH^{+}) C-LTMRs are increased in *Pten^{Het}* mutants compared to WT littermates (6.7 ±1.1% in WT vs. 21.1 ±5.1% in *Pten^{Het}*, n=5, p<0.01, Student's t-test). Quantification of IB4-positive non-peptidergic nociceptors shows no change in *Pten^{Het}* mutants compared to WT controls (32.6 ± 1.6% in WT vs. 34.7±2.5% in *Pten^{Het}*, n=5, p=0.26, Student's t-test). TrkA positive peptidergic nociceptors are decreased in *Pten^{Het}* mutants (29.4 ±2.6% in WT vs. 12.0 ±2.9% in *Pten^{Het}*, n=5, p<0.002, Student's t-test). TrkC positive (TrkC^{+}) proprioceptors were increased in *Pten^{Het}* mutants compared to WT littermates (24.4± 3.9% in WT vs. 37.0 ±3.5% in *Pten^{Het}*, n=5 p<0.02, Student's t-test).

Figure 5: Neuronal differentiation is altered in *Pten*^{Het} mutants early in development. A) Illustration of developmental landscape showing progression of DRG neuron diversification. **B-D)** Representative images of cryosections of WT and *Pten*^{Het} E11.5 DRGs with markers of each subtype (left panels) and quantification (right panels) (Scale 100 μm). **B)** Representative images of DRGs labeled with TrkA (left), quantification (right) shows a decrease in the number of TrkA positive neurons in *Pten*^{Het} mutants compared to WT littermates throughout development (n=3, E10.5: $p<0.004$; E11.5: $p<0.03$; E12.5: $p<0.02$, E13.5: $p<0.045$, E14.5: $p<0.03$, Student's t-test). **C)** Images showing DRGs labeled with TrkB (left), quantification (right) shows no changes the number of TrkB^{+} neurons in *Pten*^{Het} mutants (n=3, E10.5: $p=0.46$; E11.5: $p=0.32$; E12.5: $p=0.45$; E13.5: $p=0.47$; E14.5: $p=0.28$, Student's t-test). **D)** Images of E11.5 DRGs labeled with TrkC (left), quantification (right) shows an increase in the proportion of TrkC+ neurons in *Pten*^{Het} mutants compared to WT littermates after E10.5 (E10.5: $p<0.05$; E11.5 $p<0.05$; E12.5: $p<0.02$; E13.5: $p<0.05$; E14.5: $p<0.01$, Student's t-test).

Supplemental Figure 1: Proliferation and developmental cell death are normal in *Pten^{Het}* mutants. A) Representative images of E11.5 DRGs from WT and *Pten^{Het}* littermates birth-dated with EdU and labeled with Sox10 immunostaining (left panels) (Scale 100 μm). Quantification (right panel) shows percentage of Sox10^{+} progenitors undergoing proliferation at each developmental time point (E9.5-E14.5). At all ages quantified, there is no significant difference in the percentage of EdU^{+};Sox10^{+} precursors in *Pten^{Het}* compared to WT controls (n=3, E9.5: p=0.055; E10.5: p=0.11; E11.5: p=0.45; E12.5: p=0.06; E13.5: p=0.484; E14.5: p=0.481, at E14.5; Student's t-test). **B)** Representative images from E11.5 DRGs of WT and *Pten^{Het}* littermates showing activated Caspase 3 (Casp3; green) and Islet 1/2 immunoreactivity (left panels) (Scale 100 μm). Quantification (right panel) shows percentage of Isl1/2^{+} neurons co-labeled with activated Caspase 3. At all ages quantified (E10.5- E14.5), there is no significant difference in the percentage of activated Casp3^{+};Islet1^{+} neurons in *Pten^{Het}* DRGs compared to WT controls (n=3, E10.5: p=0.54; E11.5: p=0.16; at E12.5: p=0.069; at E13.5: p=0.91; at E14.5: p=0.84, Student's t-test).

Figure 6: *Pten* haploinsufficiency alters signaling downstream of PI3K/AKT in TrkA and TrkC lineages. A) Schematic representation of mTOR and GSK-3β signaling pathways downstream of Trk receptor activation of PI3K/AKT. **B, D-F)** Representative images of E11.5 DRGs of WT and *Pten*^{Het} littermates immunolabeled with Isl1 (B), TrkA (D), TrkB (E), TrkC (F) (orange), phospho-S6 (pS6) (purple) and GFP (green) to measure activity of the mTOR and GSK-3β/β-catenin pathways, respectively (Scale 100 μm). **C)** Quantification of Isl1^{+} neurons positive for activation of pS6 (left) and β-catenin (β-cat, right) in E11.5 DRGs from WT and *Pten*^{Het} mice. There was an increase in the proportion of pS6^{+}/Isl1^{+} neurons in *Pten*^{Het} compared to WT (28.3±4.4% in WT vs. 51.5 ±1.9 in *Pten*^{Het}, n=3, p<0.041, Student's t-test). The proportion of GFP^{+}/Isl1^{+} neurons was also increased in mutants compared to controls (23.0±0.2% in WT vs. 58.2 ±2.0 in *Pten*^{Het}, n=3, p<0.005, Student's t-test). **G)** Quantification of pS6 (left) and GFP (right) positive neurons within each DRG neuron subtype. Within the TrkA population, the pS6^{+}/TrkA^{+} neurons were increased in *Pten*^{Het} compared to WT littermates (left, 32.8±8.2% in WT vs. 66.0 ±5.1 in *Pten*^{Het}, n=3, p<0.02, Student's t-test), while there was no significant change in the number of GFP^{+}/TrkA^{+} neurons (39.7±6.9% in WT vs. 45.2 ±5.5 in *Pten*^{Het}, n=3, p=0.30, Student's t-test). Quantification in TrkB^{+} neurons shows no significant change in the proportions of pS6^{+}/TrkB^{+} neurons between *Pten*^{Het} and WT controls (39.2±14.2% in WT vs. 37.0 ±2.8 in *Pten*^{Het}, n=3, p=0.41, Student's t-test, left) or in the proportion of GFP^{+}/TrkB^{+} neurons (38.4±3.7% in WT vs. 38.2 ±0.3 in *Pten*^{Het}, p=0.96, Student's t-test). There was an increased number of pS6^{+}/TrkC^{+} neurons in *Pten*^{Het} compared to WT littermates (19.3±6.8% in WT vs. 58.2 ±13.1 in *Pten*^{Het}, n=3,

$p<0.03$, Student's t-test, left), and $GFP^+/TrkC^+$ neurons in *Pten*^{Het} compared to controls (25.2±1.5% in WT vs. 71.0 ±0.2 in *Pten*^{Het}, n=3, $p<0.002$, Student's t-test).

Figure 7: DRG neuron diversification is abnormal in *Pten*$^{Y68H/+}$ mice. A) Representative images of cryosections from WT (top) and *Pten*$^{Y68H/+}$ (bottom) P21 DRGs labeled with specific markers for select DRG subtypes (Scale 100 μm). **B)** Quantification shows subtype-specific alterations in DRG neurons in *Pten*$^{Y68H/+}$ compared to WT littermates. The proportions of CB^{+} Aβ-LTMRs and TrkB^{+} Aδ-LTMR were unchanged in *Pten*$^{Y68H/+}$ mutants, while there was a significant increase in the proportion of TH^{+} c-LTMRs (CB1: 11.2 ±3.5% in WT vs. 11.8± 1.8% in *Pten*$^{Y68H/+}$, n=3 p=0.45; TrkB: 24.1±2.9% in WT vs. 22.1±1.2% in *Pten*$^{Y68H/+}$, n=3 p=0.28; TH: 11.6±1.3% in WT vs. 23.8±1.5% in *Pten*$^{Y68H/+}$, n=3 p<0.002). There were no changes in the proportion of IB4^{+} non-peptidergic nociceptors and a significant decrease in the proportion of TrkA^{+} peptidergic nociceptors in *Pten*$^{Y68H/+}$ when compared to littermate controls (IB4: 58.1±6.9% in WT vs. 56.3±3.5% in *Pten*$^{Y68H/+}$, n=3 p=0.31; TrkA: 54.1±5.4% in WT vs. 22.7±6.0 in *Pten*$^{Y68H/+}$, n=3 p<0.01, Student's t-test). There was a significant increase in the proportion of TrkC^{+} neurons in *Pten*$^{Y68H/+}$ mutants compared to WT littermate controls (13.8±0.6% in WT vs. 34.3±2.6% in *Pten*$^{Y68H/+}$, n=3 p<0.001).

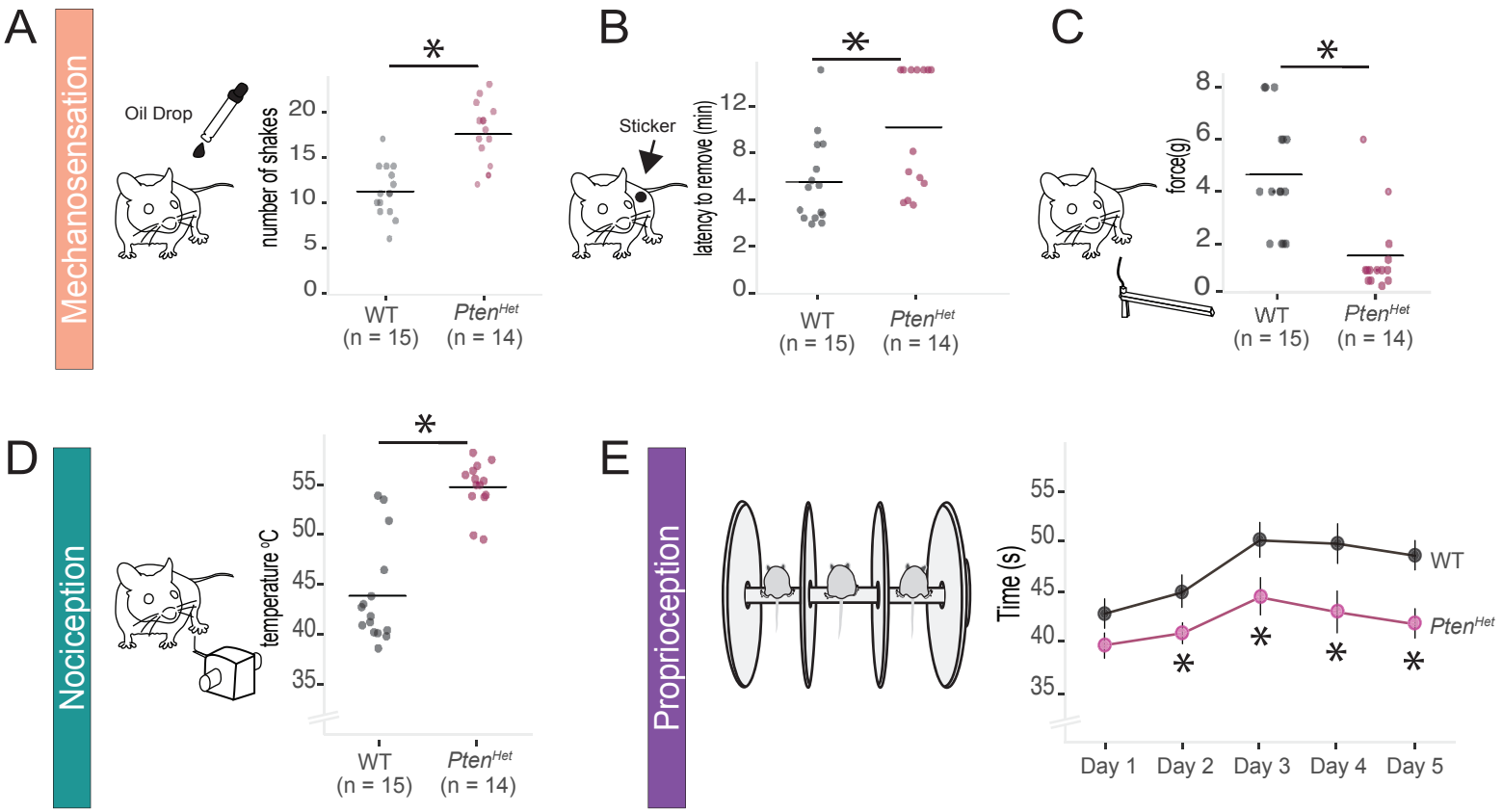
A
Mechanosensation
Oil Drop
number of shakes
20
15
10
5
0
*
WT
(n = 15)
Pten^Het
(n = 14)
B
Sticker
latency to remove (min)
12
8
4
2
0
*
WT
(n = 15)
Pten^Het
(n = 14)
C
force(g)
8
6
4
2
0
*
WT
(n = 15)
Pten^Het
(n = 14)
D
Nociception
temperature °C
55
50
45
40
35
*
WT
(n = 15)
Pten^Het
(n = 14)
E
Proprioception
Time (s)
55
50
45
40
35
WT
Pten^Het
*
*
*
*
Day 1
Day 2
Day 3
Day 4
Day 5

Figure 1

A

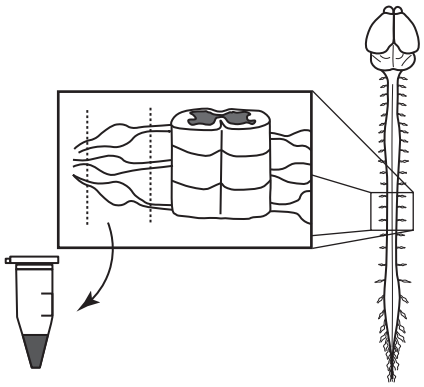

B

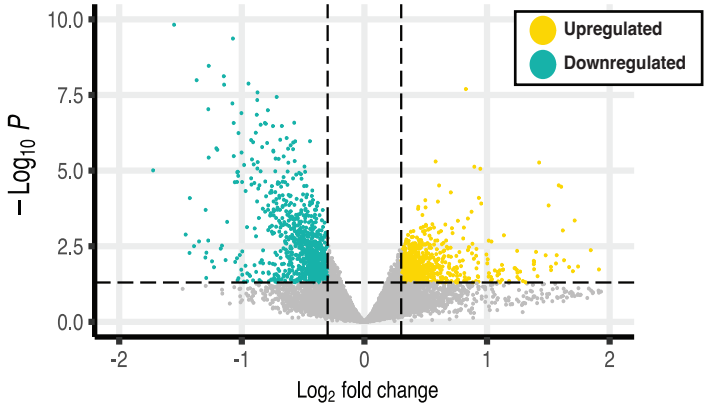

C

Upregulated	Log2 FC	p-value	adj p-value
Ddc	3.2399	0.0005	0.0329
Fsd2	1.6177	0.0009	0.0446
Zfp991	1.6051	3.42E-05	0.0044
Slc18a2	1.5845	3.08E-05	0.00423
Akr1e1	1.4780	1.06E-14	1.31E-10

Downregulated	Log2 FC	p-value	adj p-value
Mir6236	-1.7123	9.82E-06	0.0019
Rps29	-1.5528	1.51E-10	9.26E-07
Rps28	-1.3689	1.03E-08	2.10E-05
Rpl38	-1.2934	9.34E-08	8.20E-05
GM10736	-1.2707	3.72E-06	0.0009

D

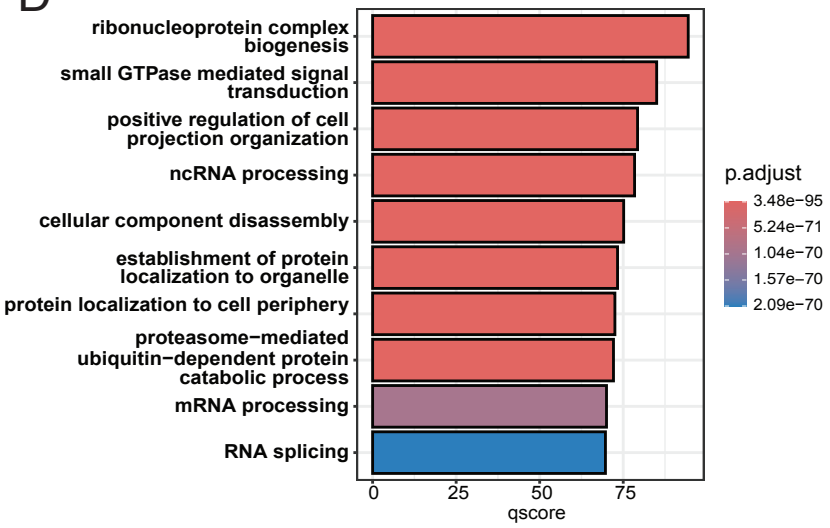

Figure 2

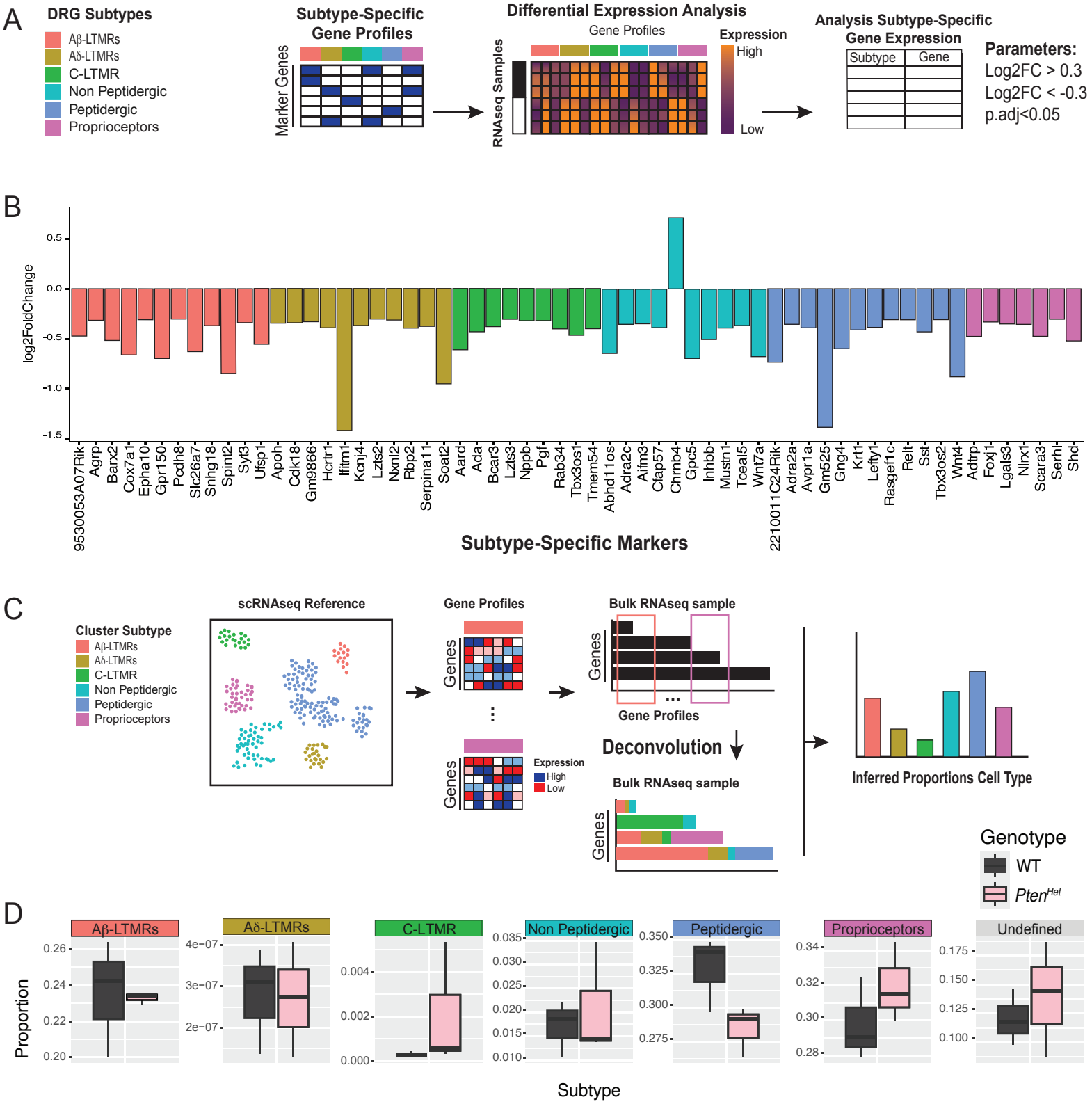
A
DRG Subtypes
Aβ-LTMRs
Aδ-LTMRs
C-LTMR
Non Peptidergic
Peptidergic
Proprioceptors
Subtype-Specific Gene Profiles
Marker Genes
Differential Expression Analysis
Gene Profiles
RNAseq Samples
Expression
High
Low
Analysis Subtype-Specific Gene Expression
Subtype
Gene
Parameters:
Log2FC > 0.3
Log2FC < -0.3
p.adj<0.05
B
log2FoldChange
0.5
0.0
-0.5
-1.0
-1.5
9530053A07Rik
Agrp
Barx2
Cox7a1
Epha10
Gpr150
Pcdh8
Slc26a7
Snhg18
Spint2
Syt3
Ufsp1
Apoh
Cdk18
Gm9866
Hcrtr1
Ifitm1
Kcnj4
Lzts2
Nxnl2
Rbp2
Serpina11
Soat2
Aard
Ada
Bcar3
Lzts3
Nppb
Pgf
Rab34
Tbx3os1
Tmem54
Abhd11os
Adra2c
Aifm3
Cfap57
Chrnb4
Gpc5
Inhbb
Mustn1
Tceal5
Wnt7a
2210011C24Rik
Adra2a
Avpr1a
Gm525
Gng4
Krt1
Lefty1
Rasgef1c
Relt
Sst
Tbx3os2
Wnt4
Adtrp
Foxj1
Lgals3
Nlrx1
Scara3
Serhl
Shd
Subtype-Specific Markers
C
Cluster Subtype
Aβ-LTMRs
Aδ-LTMRs
C-LTMR
Non Peptidergic
Peptidergic
Proprioceptors
scRNAseq Reference
Gene Profiles
Genes
Expression
High
Low
Bulk RNAseq sample
Gene Profiles
Deconvolution
Bulk RNAseq sample
Inferred Proportions Cell Type
Genotype
WT
Pten^Het
D
Aβ-LTMRs
Aδ-LTMRs
C-LTMR
Non Peptidergic
Peptidergic
Proprioceptors
Undefined
Proportion
Subtype

Figure 3

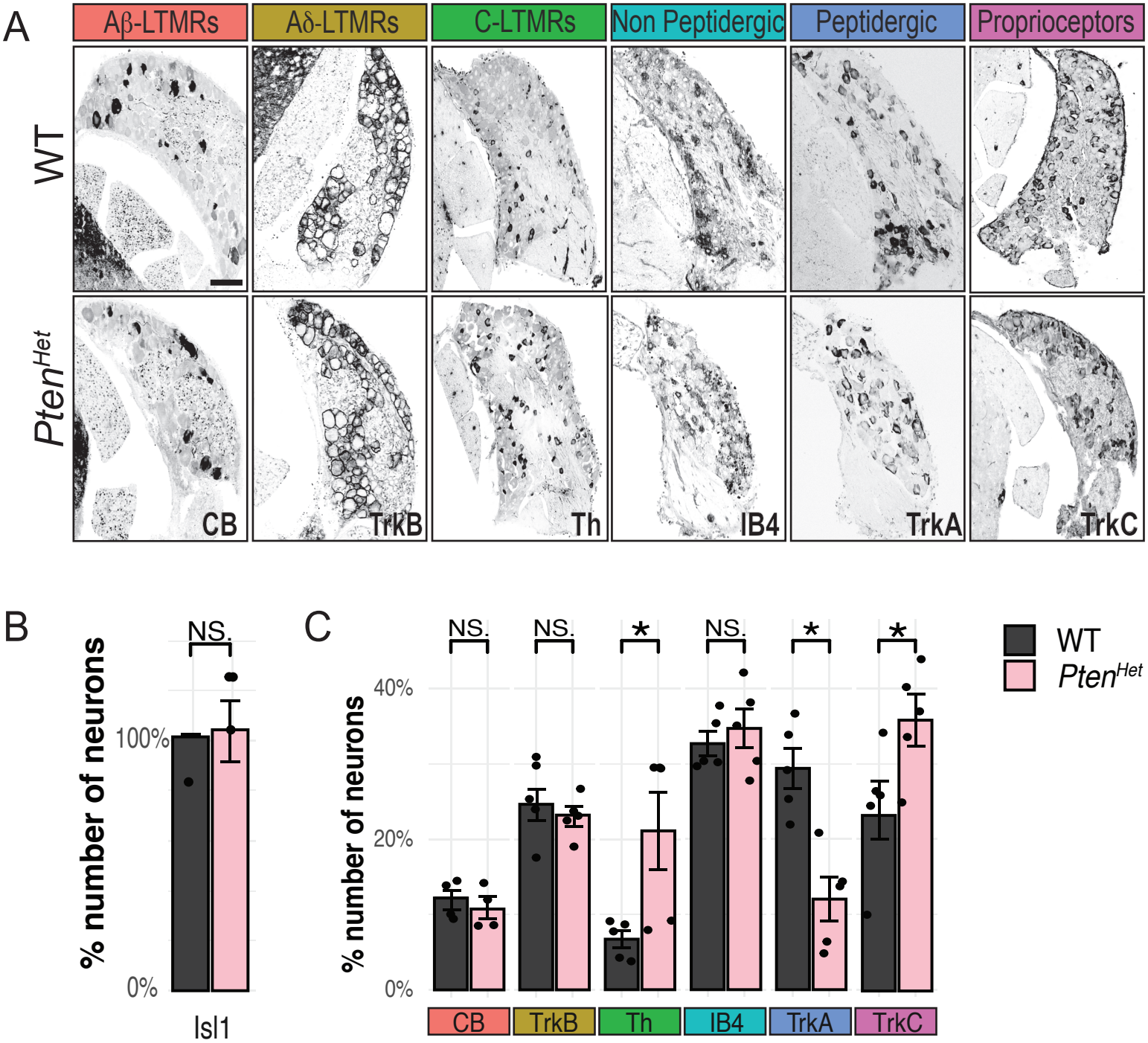
A
Aβ-LTMRs
Aδ-LTMRs
C-LTMRs
Non Peptidergic
Peptidergic
Proprioceptors
WT
PtenHet
CB
TrkB
Th
IB4
TrkA
TrkC
B
NS.
% number of neurons
100%
0%
Isl1
C
NS.
NS.
*
NS.
*
*
40%
20%
0%
CB
TrkB
Th
IB4
TrkA
TrkC
WT
PtenHet

Figure 4

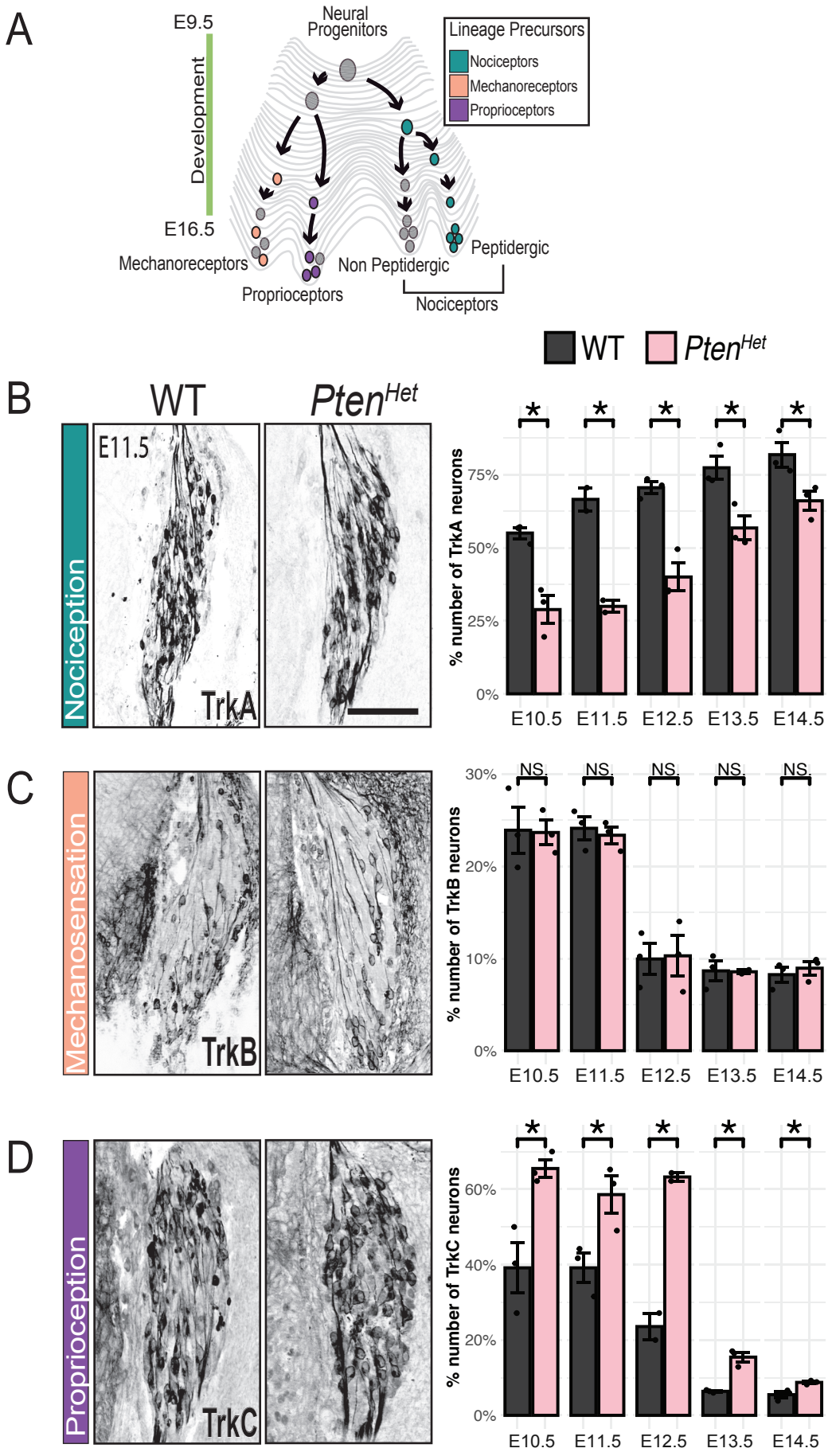
A
E9.5
Development
E16.5
Neural Progenitors
Lineage Precursors
Nociceptors
Mechanoreceptors
Proprioceptors
Mechanoreceptors
Proprioceptors
Non Peptidergic
Peptidergic
Nociceptors
WT
PtenHet
B
WT
PtenHet
Nociception
E11.5
TrkA
% number of TrkA neurons
75%
50%
25%
0%
E10.5
E11.5
E12.5
E13.5
E14.5
C
Mechanosensation
TrkB
% number of TrkB neurons
30%
20%
10%
0%
NS.
D
Proprioception
TrkC
% number of TrkC neurons
60%
40%
20%
0%

Figure 5

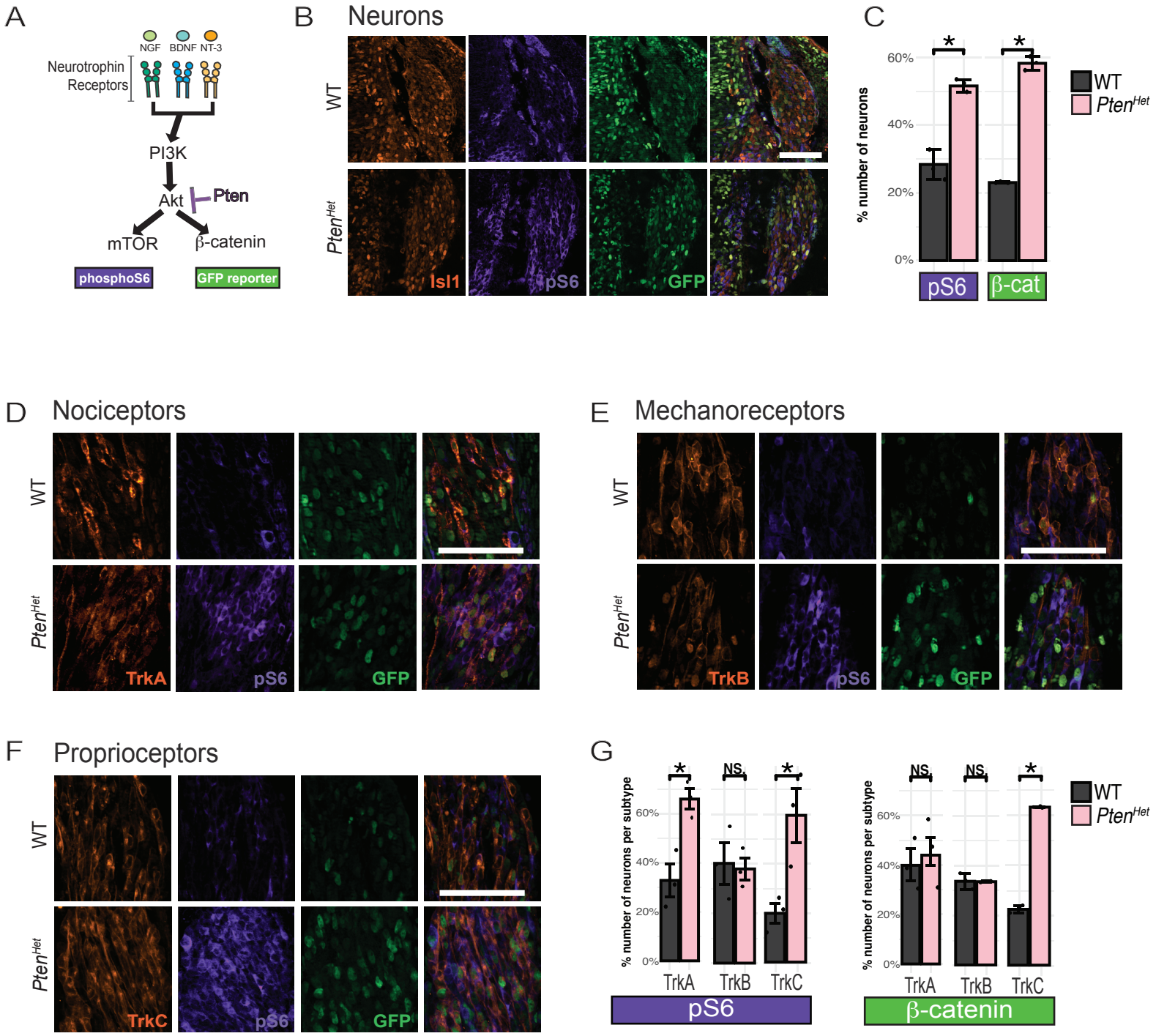
A
NGF
BDNF
NT-3
Neurotrophin Receptors
PI3K
Akt
Pten
mTOR
β-catenin
phosphoS6
GFP reporter
B
Neurons
WT
PtenHet
Isl1
pS6
GFP
C
% number of neurons
60%
40%
20%
0%
WT
PtenHet
pS6
β-cat
D
Nociceptors
WT
PtenHet
TrkA
pS6
GFP
E
Mechanoreceptors
WT
PtenHet
TrkB
pS6
GFP
F
Proprioceptors
WT
PtenHet
TrkC
pS6
GFP
G
% number of neurons per subtype
60%
40%
20%
0%
NS
TrkA
TrkB
TrkC
pS6
β-catenin
WT
PtenHet

Figure 6

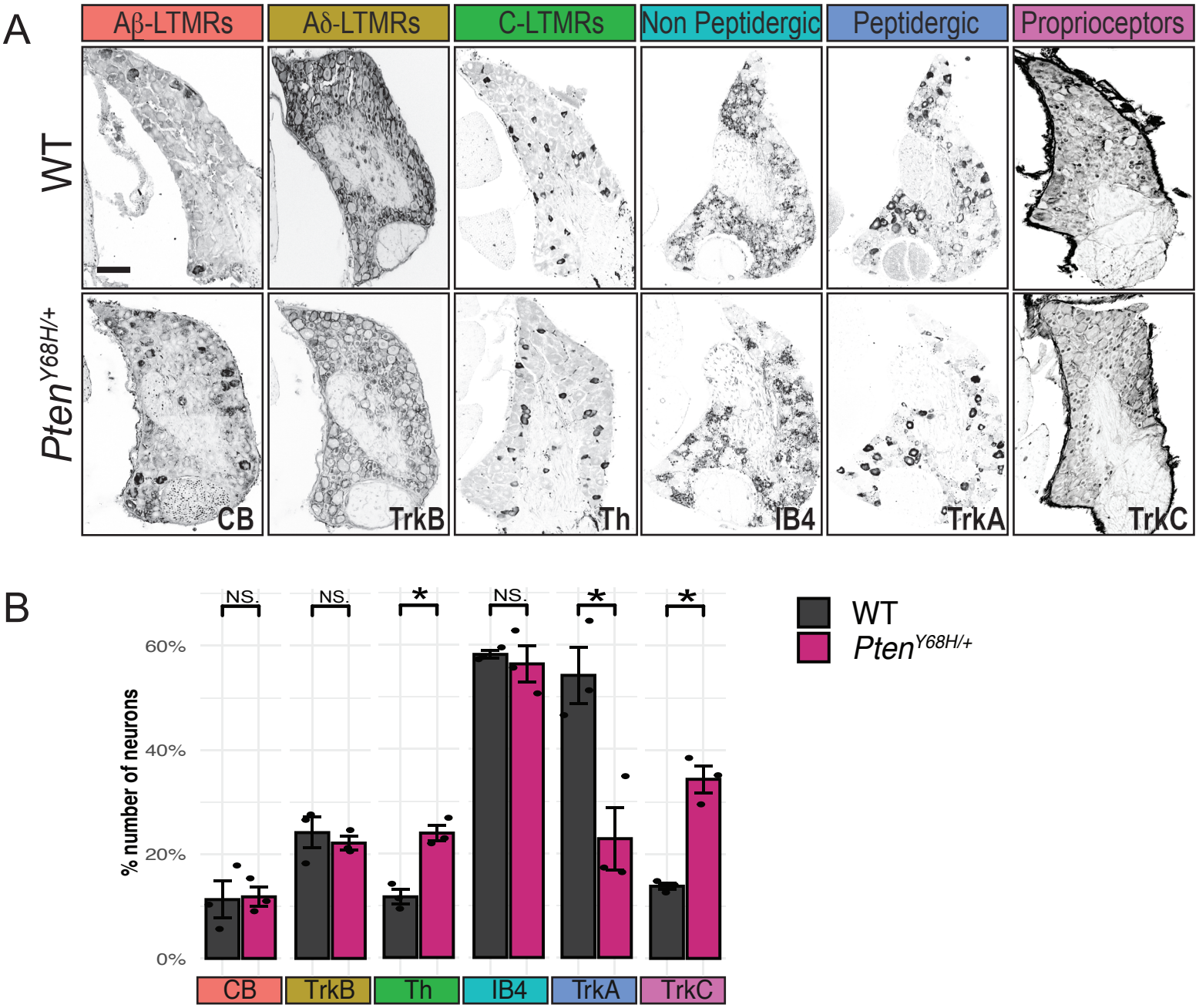
A
Aβ-LTMRs
Aδ-LTMRs
C-LTMRs
Non Peptidergic
Peptidergic
Proprioceptors
WT
Pten Y68H/+
CB
TrkB
Th
IB4
TrkA
TrkC
B
NS.
NS.
*
NS.
*
*
WT
Pten Y68H/+
% number of neurons
60%
40%
20%
0%
CB
TrkB
Th
IB4
TrkA
TrkC

Figure 7

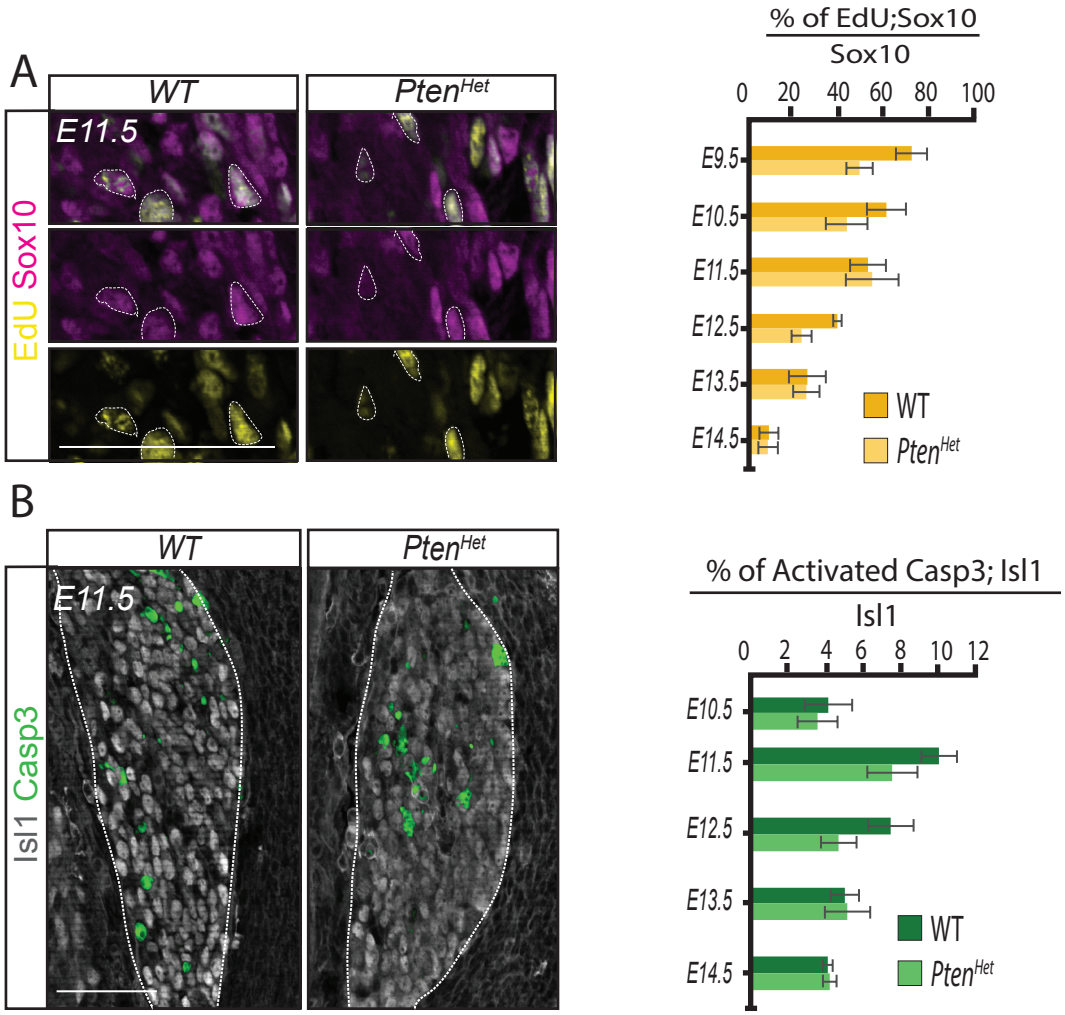
A
WT
Pten^Het
E11.5
EdU Sox10
% of EdU;Sox10
Sox10
0 20 40 60 80 100
E9.5
E10.5
E11.5
E12.5
E13.5
E14.5
WT
Pten^Het
B
WT
Pten^Het
E11.5
Isl1 Casp3
% of Activated Casp3; Isl1
Isl1
0 2 4 6 8 10 12
E10.5
E11.5
E12.5
E13.5
E14.5
WT
Pten^Het

Figure S1